Phase diagrams of hard-core repulsive Yukawa particles

Antti-Pekka Hynninen and Marjolein Dijkstra
Debye Institute, Soft Condensed Matter Physics, Utrecht University, Princetonplein 5, 3584 CC Utrecht, The Netherlands
(Received 2 April 2003; published 19 August 2003)

We determine the phase behavior of hard spheres interacting with repulsive Yukawa (screened Coulomb) interaction using computer simulations. We study the effect of the hard-core diameter on the phase behavior of repulsive Yukawa particles by comparing our phase diagrams with that of repulsive point Yukawa particles. We show that for sufficiently high contact values of the pair potential ($\beta\epsilon=20$, 39, 81, and higher), the fluid-face-centered-cubic (fcc) solid, at high screening, the fluid-body-centered-cubic (bcc) solid and the bcc-fcc coexistence for packing fractions $\eta\lesssim 0.5$ are well described by the phase boundaries of point Yukawa particles, by employing a mapping of the point Yukawa system onto a hard-core repulsive Yukawa system. While the bcc-fcc coexistence is well described by the point Yukawa limit for $\eta<0.5$, we find a deviation at higher η as the hard-core repulsion favors the fcc solid for $\eta\geqslant 0.5$, independent of the screening. Consequently, a second triple point appears in the phase diagram in the weak screening regime. In addition, we find that all the phase coexistence regions in our phase diagrams for hard-core repulsive Yukawa system are very narrow, i.e., a small density jump in the coexisting phases.

DOI: 10.1103/PhysRevE.68.021407 PACS number(s): 82.70.Dd, 64.70.−p, 64.60.Cn

I. INTRODUCTION

Particles whose interactions are described by the repulsive Yukawa (screened Coulomb) pair potential can be used to model various physical systems including elementary particles, small charged ''dust'' grains observed in plasma environments, and suspensions of charge-stabilized colloids. Our interest lies especially in the phase behavior of the last example, i.e., colloids. In what follows, since there is no danger of misinterpretation, we refer to ''repulsive Yukawa potential'' simply as ''Yukawa potential.''

Charge-stabilized colloidal suspensions consist of spherical or anisotropic mesoscopic colloidal particles suspended in a polar solvent with coions and counterions. A direct treatment of the full problem, including the microscopic coions and counterions and the mesoscopic colloids, is, in most cases, impractical due to a large gap between the length and time scales involved for the various species. Therefore, most studies on charge-stabilized colloids are based on models in which the degrees of freedom of the microscopic particles have been integrated out such that the mesoscopic particles interact with an effective potential. The standard way to do this coarse graining to an effective one-component system is due to the seminal work of Derjaguin, Landau, Verwey, and Overbeek, which is known as the DLVO theory after them [1]. The DLVO theory predicts that the effective pair interaction between the colloids consists of a hard-core repulsion due to the finite size of the colloids, screened-Coulomb (Yukawa) repulsion with the screening length given by the Debye length κ^{-1} of the electrolyte, and van der Waals attractions with a typical range of a few nm. The screening length κ^{-1} defines the thickness of the double layer of opposite charge surrounding each colloidal surface. Range κ^{-1} of the screened-Coulomb repulsion is a function of the salt concentration of the electrolyte, the dielectric constant of the solvent, and the temperature. In most situations the van der Waals attractions can be neglected and one ends up with a model for the colloid-colloid interaction that is given by the hard-core Yukawa potential.

The phase diagram of point Yukawa particles is known from earlier studies [2,3]. While the small dust grains can be thought of as being pointlike, i.e., without physical dimensions, the same is not outright true for colloidal particles with a mesoscopic diameter. Intuitively, two limiting cases for the effect of the hard core can be considered.

(i) In the limit of highly charged colloids, or low density of colloids (or both), the particles hardly ever come close enough to touch each other and therefore, the effect of the hard-core diameter is minimal.

(ii) Analogously, in the other extreme of low charge, or high density (or both), the hard-core interaction should play a large role. However, in order to make a more precise analysis, we decide to study the phase behavior of hard-core Yukawa particles systematically.

Phase diagram of hard-core Yukawa particles has been earlier studied in Refs. [4,5]. These earlier studies have, in many ways, inspired our work: Not only do we use similar methods but also directly utilize the data given in them. Among other things studied in Ref. [5], a full phase diagram was presented for one contact value $\beta\epsilon=8$ and also some comparison with point Yukawa particle results was made. We extend this study by calculating phase diagrams for several values of $\beta\epsilon$ and perform a mapping between the hard-core Yukawa and the point Yukawa systems. Our main conclusion is that the phase diagram of hard-core repulsive Yukawa particles can be obtained for any contact value $\beta\epsilon$ which is sufficiently high ($\beta\epsilon=20$ or higher), by mapping the well-known phase boundaries of the point Yukawa system onto those of the hard-core repulsive Yukawa system and using that the stable bcc region is bounded by a bcc-fcc coexistence at $\eta\approx 0.5$, i.e., the hard-core repulsion favors the fcc phase for $\eta>0.5$.

This paper is organized as follows. In Sec. II we describe the model and the methods which are used to determine the phase behavior of the hard-core Yukawa particles. In Sec. III

we present the results, compare them to earlier results of point Yukawa particles, and give technical details regarding the calculations, and finally, in Sec. IV, we conclude.

II. MODEL AND METHODS

Our model consists of particles interacting with the pairwise repulsive Yukawa potential, which includes the hard-core interaction. This means that the pair potential is given by

$$\beta u(r)=\begin{cases}\beta\epsilon\dfrac{\exp[-\kappa\sigma(r/\sigma-1)]}{r/\sigma}, & r>\sigma\\ \infty, & r<\sigma,\end{cases} \tag{1}$$

where $\beta\epsilon$ is the value of the pair potential at contact per k_BT, κ is the inverse Debye screening length, and σ is the hard-core diameter. Note that with the help of the DLVO pair potential, the contact value can be written as

$$\beta\epsilon=\frac{Z^2}{(1+\kappa\sigma/2)^2}\frac{\lambda_B}{\sigma}, \tag{2}$$

where Z is the charge of the colloids and $\lambda_B=\beta e^2/\epsilon_s$ is the Bjerrum length of the solvent with dielectric constant ϵ_s [1]. The total potential energy of N particles is given by the sum over all pairs, i.e.,

$$U(\mathbf{r}^N)=\sum_{i<j}^{N} u(r_{ij}). \tag{3}$$

In most experiments on charge-stabilized colloidal suspensions, one makes several assumptions for charge Z and the inverse Debye screening length $\kappa\sigma$. Charge Z is often replaced by a so-called renormalized or saturated charge that depends both on $\kappa\sigma$ and on the packing fraction $\eta=\pi/6\sigma^3N/V$ [6,7]. Furthermore, one often considers a $\kappa\sigma$ that depends on Z, η, and on the added salt concentration [8]. This means that the relationship between $\beta\epsilon$, $\kappa\sigma$, and η is complicated. However, an η and Z independent $\kappa\sigma$ can be realized by coupling the system to a salt reservoir and considering $\kappa\sigma$ to be that of the reservoir. In addition, we take the value of $\beta\epsilon$ to be fixed, which can later be related to experimental system parameters through Eq. (2). In this way, $\beta\epsilon$ and $\kappa\sigma$ are independent variables, i.e., independent of each other and of the colloid packing fraction η, and we calculate the phase behavior in the three dimensional space spanned by them. This means that two phases in coexistence have, as usual, equal pressure p and equal chemical potential μ, but have also equal $\kappa\sigma$ and equal $\beta\epsilon$, while η is different.

Our purpose is to use a combination of Helmholtz free energy calculations and the so-called Kofke integration method [9] to trace out the phase diagram of the hard-core Yukawa particles. Similar method has already been used to study the phase diagram of the hard-core Yukawa particles in Refs. [4,5]. The phase diagram consists of stable regions of the fluid, bcc, and fcc phases that are bounded by coexistence regions between any two phases. Therefore, the determination of the phase diagram reduces to the calculation of the coexistence lines. Points on the coexistence line can be determined by calculating, for each phase, the Helmholtz free energy per volume as a function of density and using the common tangent construction to obtain the densities of the coexisting phases. In principle, this could be repeated for every point to obtain a smooth coexistence line. However, this would be computationally very demanding and, as it turns out, not even necessary. The reason for this is that once one point on the coexistence line is known, the rest of the line can be calculated without performing additional free energy calculations. This can be achieved by employing a numerical method first proposed by Kofke [9]. We are interested in calculating the phase coexistence lines in the $(\eta,\kappa\sigma)$ plane for a fixed $\beta\epsilon$. In this case, Kofke's method amounts to integrating

$$dp=-\frac{\langle\beta U'/N\rangle_1-\langle\beta U'/N\rangle_2}{\langle V/N\sigma^3\rangle_1-\langle V/N\sigma^3\rangle_2}d(\kappa\sigma) \tag{4}$$

(for the derivation, see Ref. [5]) from a known starting point $(p,\kappa\sigma)$. Note that the two phases in coexistence have the same p, $\beta\epsilon$, and $\kappa\sigma$ but different η. In Eq. (4), $p=\beta P\sigma^3$ is the dimensionless pressure, $\langle\cdots\rangle_i$ denotes ensemble average of the ith phase $(i=1,2)$, and U' is the partial derivative of the total potential energy with respect to $\kappa\sigma$.

In practice, Eq. (4) is integrated as follows. Differentials dp and $d(\kappa\sigma)$ are replaced by finite differences Δp and $\Delta(\kappa\sigma)$. Starting from a known coexistence point with p and $\kappa\sigma$, Monte Carlo (MC) simulations [10] are performed for both the phases in the NPT (isobaric) ensemble to calculate the ensemble averages in Eq. (4). This gives us a prediction for the slope in the coexistence line in the $(p,\kappa\sigma)$ plane. Changing $\kappa\sigma$ to $\kappa\sigma+\Delta(\kappa\sigma)$, we perform MC simulations for both the phases at pressure $p+\Delta p$ predicted by Eq. (4) and we calculate again the ensemble averages in Eq. (4). Continuing in this manner gives us a series of points $\{p_j,(\kappa\sigma)_j\}$ that lie on the coexistence line. At each point the packing fractions of the two phases are determined using the ensemble averages $\eta_i=\pi/6\sigma^3N/\langle V\rangle_i$, obtained from the NPT simulations.

The practical limitation of this method is that there is no inherent mechanism that guarantees that we stay on the coexistence line. In other words, during the integration of Eq. (4), numerical errors may accumulate to yield large deviations from the actual coexistence line. This problem can be avoided by employing a more sophisticated version of the method by Meijer and El Azhar, where additional free energy calculations are used to fix the estimates of the coexisting points [4]. However, instead of implementing the method of Meijer and El Azhar, we decided to check the stability of the Kofke integration by performing separate free energy calculations at a couple of points along the coexistence line. The difference between the results from the free energy and Kofke integration gives us an idea of the total numerical error accumulated. To calculate the Helmholtz free energy, we use the so-called λ integration for the fluid phase and Frenkel-Ladd method for the crystal phases [10,11].

In order to compare our results for hard-core Yukawa particles to the earlier results obtained for point Yukawa particles [2,3], we need to define a mapping between the two systems. A natural choice for this mapping is to equate the two Yukawa potentials outside the hard core. However, since the results for the point Yukawa particle phase diagrams are typically presented in units different than those for the hard-core Yukawa particles, we have to explain the situation a little further.

In the case of point Yukawa particles, the relevant length scale is the characteristic interparticle separation $a=\rho^{-1/3}$. Once a is chosen as the length scale, the pair potential describing the point Yukawa particles can be written as

$$\beta u(r)=\beta U_0\frac{\exp(-\lambda r/a)}{r/a}, \tag{5}$$

where βU_0 is a constant prefactor and λ is the inverse of the screening length in units of a. While the phase space of hard-core Yukawa particles is three dimensional ($\beta\epsilon$, $\kappa\sigma$, and η), only two independent variables exist in the case of point Yukawa particles; since a is chosen as the length scale, there is no need for a density axis. We are therefore left with a two dimensional phase space consisting of prefactor βU_0 and the inverse screening length λ. Setting the two pair potentials in Eqs. (1) and (5) to be equal for $r>\sigma$ results in two equations given by

$$\kappa=\lambda/a,$$

$$e^{\kappa\sigma}\sigma\beta\epsilon=\beta U_0 a. \tag{6}$$

The first line of Eq. (6) results from setting the exponential decays of the two pair potentials to be equal and the second from the equality of the prefactors. Using the fact that $a=(6\eta/\pi)^{-1/3}\sigma$, we can rewrite Eq. (6) as

$$\beta U_0=e^{\kappa\sigma}\beta\epsilon(6\eta/\pi)^{1/3},$$

$$\lambda=\kappa\sigma(6\eta/\pi)^{-1/3}. \tag{7}$$

Equation (7) can be used to map a phase diagram of hard-core Yukawa particles to a phase diagram of point Yukawa particles, and vice versa.

As mentioned above, the phase diagram of the point Yukawa particles can be given in terms of the inverse screening length λ and prefactor βU_0. This is what we call the $(\lambda,\beta U_0)$ representation. Another representation of the point Yukawa phase diagram is the $(\lambda,\tilde{T})$, where

$$\tilde{T}=\left[\frac{2}{3}\lambda^2\beta U_0 u_M(\lambda)\right]^{-1} \tag{8}$$

is the dimensionless temperature and where u_M is the Madelung energy of a fcc crystal (i.e., the potential energy of an ideal crystal) per particle per βU_0 [2,3]. The $(\lambda,\tilde{T})$ representation is convenient since it leads to phase boundaries that are almost straight lines. In Ref. [3], the results for the fluid-bcc and fluid-fcc melting lines and the bcc-fcc phase boundary are given as polynomial fits in the $(\lambda,\tilde{T})$ plane. We give fits here for the phase boundaries of point Yukawa particles in the $(\lambda,\beta U_0)$ plane using the results of Ref. [3], as this representation does not include the more elaborate Madelung energy calculation. The fluid-bcc phase boundary is well fitted by

$$\begin{aligned}\ln(\beta U_0)=&\,4.670-0.041\,71\lambda+0.1329\lambda^2-0.010\,43\lambda^3\\&+4.343\times10^{-4}\lambda^4\\&-6.924\times10^{-6}\lambda^5,\quad \text{for}\ \ 0\leqslant\lambda\leqslant12,\end{aligned} \tag{9}$$

while the fit of the bcc-fcc phase boundary is given by

$$\begin{aligned}\ln(\beta U_0)=&\,97.651\,06-150.469\,699\lambda+106.626\,405\lambda^2\\&-41.671\,36\lambda^3+9.639\,931\lambda^4-1.315\,024\,9\lambda^5\\&+0.097\,848\,11\lambda^6\\&-0.003\,063\,96\lambda^7,\quad \text{for}\ \ 1.85\leqslant\lambda\leqslant6.8.\end{aligned} \tag{10}$$

Together with Eq. (7), the fits in Eqs. (9) and (10) enable us to map the phase diagram of point Yukawa particles onto any hard-core Yukawa system.

NPT and *NVT* MC simulations, needed in the Kofke integration and free energy calculations, were carried out in a cubic box (with few exceptions) and with periodic boundary conditions. The cutoff radius of the potential was always chosen to be half of the box length and a continuous distribution of particles beyond the cutoff was assumed for the tail correction of the total potential energy [10]. In the limit of weak screening $\kappa\sigma\ll1$, the use of cutoffs in the potential is inaccurate, as the range of the potential is larger than half of the box length. This problem can be fixed by using Ewald summation adapted for Yukawa interactions [12], or by applying the method elaborated in Ref. [13], where spline functions are used to approximate the effective interactions that result from taking into account all image particles. In the current case, it is, however, sufficient to limit ourselves in the regime $\kappa\sigma\geqslant2.0$, where the effects of the finite cutoff remain small or can be eliminated by moderately increasing the system size. We believe that the essential results remain the same although, with the inclusion of noncut potentials, the error bars could be made smaller.

III. RESULTS

Using the methods described in Sec. II, we study the phase behavior of hard-core Yukawa particles, whose interactions are described by the pair potential given by Eq. (1). The phase diagrams are calculated for fixed contact values $\beta\epsilon$ and they are given in the $(\eta,1/\kappa\sigma)$ representation. We calculate the phase diagram for four contact values, $\beta\epsilon=8$, 20, 39, and 81, and the results are given in Figs. 1, 2, 3, and 4, respectively. In all the four phase diagrams the gray areas bounded by the solid lines give the coexistence regions (tie lines are horizontal), while the dashed lines give the point Yukawa phase boundaries of Ref. [3]. The mapping needed to plot the point Yukawa results was discussed in Sec. II. This section is organized in two parts: First we present the

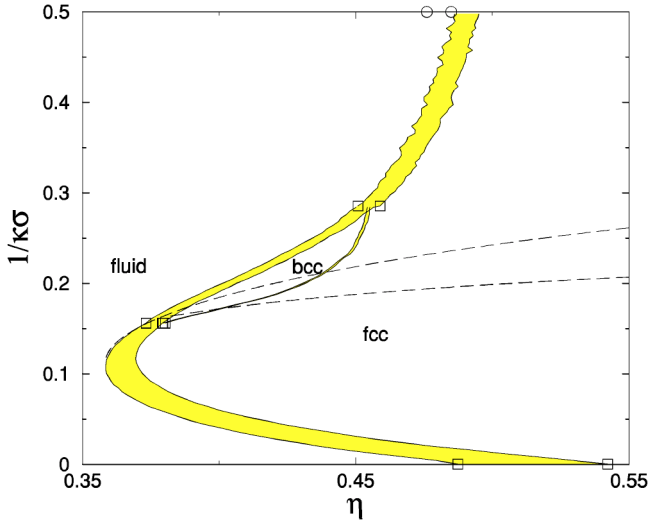

FIG. 1. Phase diagram for a system in which the particles interact via a hard-core repulsive Yukawa pair potential Eq. (1) with $\beta\epsilon=8$ presented in the (packing fraction η, Debye screening length $1/\kappa\sigma$) plane. In charge-stabilized colloidal suspensions, the lower part of the diagram ($1/\kappa\sigma=0$) is a high salt regime and the upper part ($1/\kappa\sigma=0.5$) is a low salt regime. The solid lines are coexistence lines obtained by using the Kofke integration and the gray areas denote the coexistence regions. The tie lines are horizontal. We find a stable fluid phase at low η, a stable face-centered-cubic (fcc) solid at high η, and in between, a stable body-centered-cubic (bcc) solid. The dashed lines are the phase boundaries of the point Yukawa particles by Hamaguchi, Farouki, and Dubin [3]. The squares (□) mark the starting points for the Kofke integration and the circles (○) are checkup points for the coexistence that were obtained using free energy calculations.

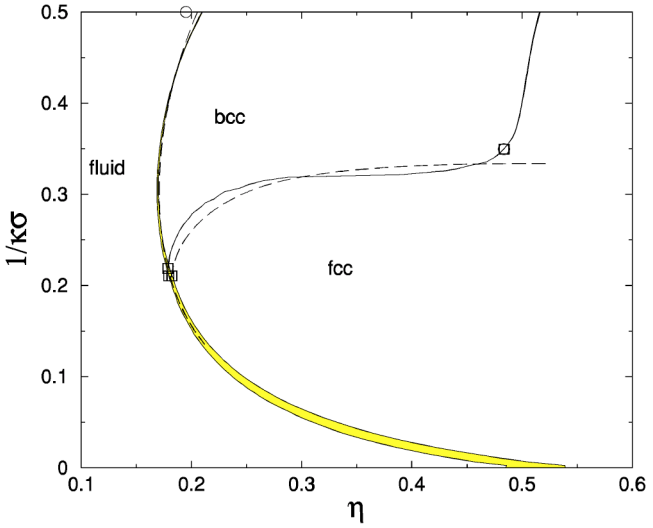

FIG. 3. Phase diagram for a system in which the particles interact via a hard-core repulsive Yukawa pair potential Eq. (1) with $\beta\epsilon=39$ presented in the $(\eta,1/\kappa\sigma)$ plane. The symbols and lines are the same as in Fig. 1. Note the difference in the η scale, compared to Figs. 1, 2, and 4.

results and second, we give technical details regarding the calculations.

Let us first describe the structure of the phase diagrams in Figs. 1–4. The phase diagrams start from the hard-sphere limit at $1/\kappa\sigma=0$ with coexisting fluid and fcc phases at packing fractions $\eta=0.491$ and $\eta=0.543$, respectively. As the softness and the range of the interactions increase with increasing screening length $1/\kappa\sigma$, the fluid-fcc coexistence becomes thinner and moves to lower packing fractions, in agreement with Ref. [14]. A further increase of $1/\kappa\sigma$ takes us to the fluid-bcc-fcc triple point. Here, the softness and the

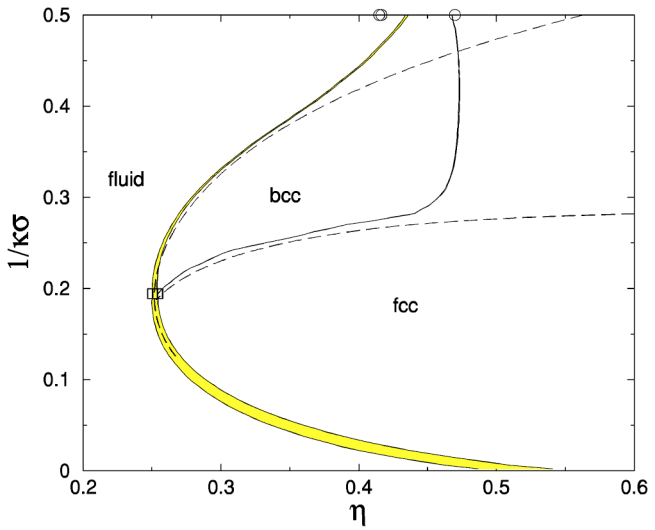

FIG. 2. Phase diagram for a system in which the particles interact via a hard-core repulsive Yukawa pair potential Eq. (1) with $\beta\epsilon=20$ presented in the $(\eta,1/\kappa\sigma)$ plane. The symbols and lines are the same as in Fig. 1. Note the difference in the η scale, compared to Figs. 1, 3, and 4.

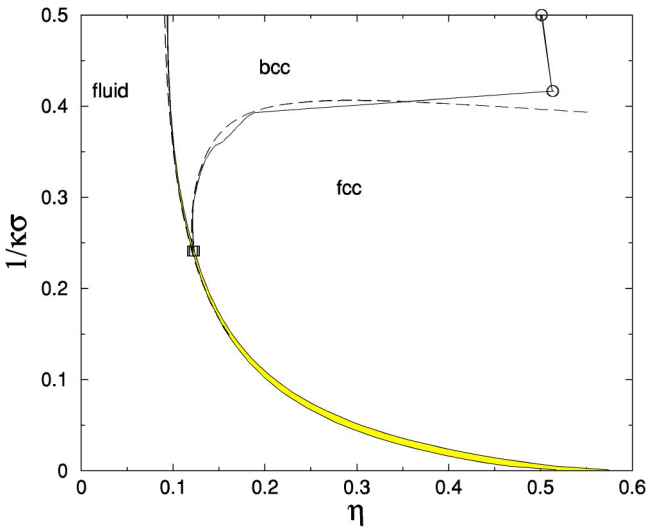

FIG. 4. Phase diagram for a system in which the particles interact via a hard-core repulsive Yukawa pair potential Eq. (1) with $\beta\epsilon=81$ presented in the $(\eta,1/\kappa\sigma)$ plane. The symbols and lines are the same as in Fig. 1. Note the difference in the η scale, compared to Figs. 1, 2, and 3.

range of the interactions are so pronounced that at lower packing fractions it is more favorable to form a bcc crystal than a fcc crystal.

Increasing $1/\kappa\sigma$ from the triple point, two phase coexistence lines originate, namely, the fluid-bcc and the bcc-fcc. While the fluid-bcc coexistence line is relatively smooth, the bcc-fcc line moves quickly to higher packing fraction, producing a broad region of stable bcc phase. This is especially true for $\beta\epsilon=20$, 39, and 81 (Figs. 2–4), and we can see that the steepness of this ''shootup'' behavior becomes more pronounced with large $\beta\epsilon$. After the shootup, at higher values of $1/\kappa\sigma$, the bcc-fcc coexistence line turns and behaves more or less as a straight vertical line at $\eta\approx0.5$. At high $1/\kappa\sigma$ the fluid-bcc coexistence line turns to higher packing fractions, i.e., here the fluid phase becomes more favorable with respect to the bcc phase. A simple explanation for this is that at high $1/\kappa\sigma$, where the range of interactions becomes longer than the average interparticle spacing in the crystal, the importance of the repulsive bonds needed to form the bcc crystal vanishes. Since in this case both the fluid and the bcc phases have a similar energetic contribution to the free energy, the fluid phase wins since it has larger entropy.

It is worthwhile to note that in all the phase diagrams in Figs. 1–4, both the fluid-bcc and the bcc-fcc coexistence regions are very narrow, or in other words, the density difference between the two phases is small. In particular, the bcc-fcc coexistence region is extremely narrow: The density jump between the bcc and the fcc phases is the largest for $\beta\epsilon=8$, where it is less than 0.3% [15]. Therefore, it is surprising that some experiments on charge stabilized colloids report on (broad) bcc-fcc coexistence, i.e., they are able to have measurement points well inside the bcc-fcc coexistence region [16,17].

In the case of the lowest contact value $\beta\epsilon=8$ (Fig. 1), the bcc region ends at another triple point around $1/\kappa\sigma=0.28$, at higher $1/\kappa\sigma$, fluid-fcc coexistence continues. The presence of the second triple point for the hard-core Yukawa particles has already been found in Ref. [5], where the phase diagram for $\beta\epsilon=8$ was presented. The tendency of the bcc region to close up can also be seen in the phase diagram for $\beta\epsilon=20$ (Fig. 2), where the fluid-bcc and the bcc-fcc coexistence lines turn towards each other at around $1/\kappa\sigma=0.5$. Note also that this tendency moves to higher $1/\kappa\sigma$ with increasing contact value $\beta\epsilon$. Based on our results, we expect another triple point for all $\beta\epsilon$ at high values of $1/\kappa\sigma$, although our calculations could only reach it at $\beta\epsilon=8$. We also predict that with increasing $\beta\epsilon$, this other triple point escapes very quickly to high values of $1/\kappa\sigma$, i.e., to the regime where numerical calculations are difficult to carry out.

In Fig. 5 we summarize the results from Figs. 1–4 by plotting all the phase diagrams in one figure. We observe from Fig. 5 that the low $1/\kappa\sigma$ triple point moves to lower η and higher $1/\kappa\sigma$ with increasing contact value $\beta\epsilon$. Another observation is that the region of stable bcc phase broadens, mainly because the fluid-bcc coexistence line moves to lower packing fractions, while the bcc-fcc coexistence line moves only slightly to higher η and seems to saturate around $\eta\gtrsim0.5$. We discuss the dashed line connecting the triple points in Fig. 5 later.

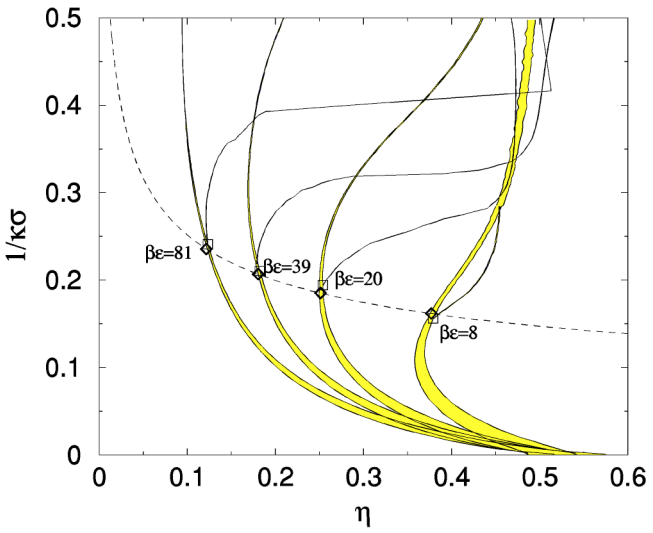

FIG. 5. Phase diagrams of Figs. 1–4 plotted in one figure. The dashed line gives the line of triple points predicted by the point Yukawa results of Hamaguchi, Farouki, and Dubin [3], the diamonds (◇) highlight the triple points at $\beta\epsilon=8$, 20, 39, and 81, and the squares (□) mark the position of the triple points used in our calculations.

We now turn our attention to a comparison of our results on hard-core Yukawa particles with those obtained for point Yukawa particles by Hamaguchi, Farouki, and Dubin [3]. Note that the calculations of Hamaguchi, Farouki, and Dubin did not include the determination of the phase coexistence regions. Therefore, in the case of point Yukawa particles, we can only talk about phase boundaries. In Figs. 1–4 these phase boundaries are plotted with dashed lines. Figures 1–4 show that the phase boundaries of hard-core Yukawa particles approach those of the point Yukawa particles with increasing $\beta\epsilon$. This is due to the fact that at high values of $\beta\epsilon$ the particles hardly ever get close enough to feel the hard-core interaction. In the case of charge-stabilized colloidal suspensions, high $\beta\epsilon$ corresponds to highly charged colloids [see Eq. (2)]. The deviation between the point and hard-core Yukawa results is particularly pronounced in the case of $\beta\epsilon=8$ (Fig. 1). For the rest of the phase diagram with higher $\beta\epsilon$, the description with point Yukawa particles improves. Especially, the fluid-fcc line at high $1/\kappa\sigma$, the fluid-bcc line as well as the beginning of the bcc-fcc line are well predicted by the point Yukawa picture. However, the vertical rise of the bcc-fcc line at high $1/\kappa\sigma$ is completely missing in the point Yukawa phase diagram. Instead, the bcc region is predicted to become indefinitely broad in the point Yukawa limit, hindering the possibility of a second triple point. Thus, we see that the closing of the bcc region by a second triple point is caused solely by the presence of the hard-core interaction.

Next, we make a small excursion to study the position of the low $1/\kappa\sigma$ triple point. In the case of point Yukawa particles, the position of the triple point is at $\lambda^{\mathrm{tp}}=6.90$ and $\beta U_0^{\mathrm{tp}}=3474$ [3]. We can map this point to any hard-core Yukawa system by using Eq. (7). More specifically, we can solve the triple point $\kappa\sigma$ for fixed $\beta\epsilon$ from

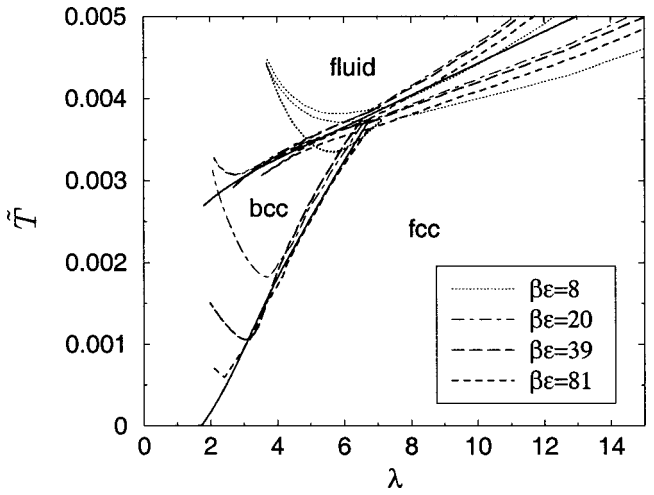

FIG. 6. Phase diagram in the $(\lambda,\tilde{T})$ representation. The solid lines are point Yukawa results of Hamaguchi, Farouki, and Dubin [3] and the rest of the lines are our hard-core Yukawa results $\beta\epsilon=8$, 20, 39, and 81 using the mapping discussed in the text. For clarity, the coexistence regions of the hard-core Yukawa results are left unfilled and only the coexistence lines are drawn.

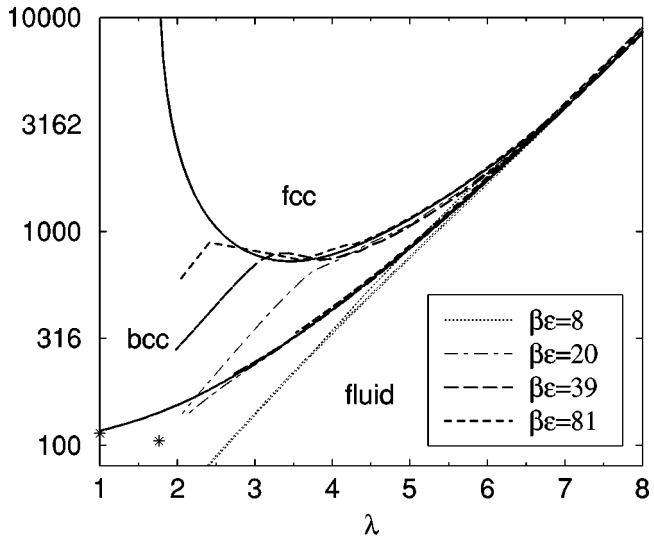

FIG. 7. Phase diagrams in the $(\lambda,\beta U_0)$ representation plotted in linear-log scale. The lines are the same as in Fig. 6 and the stars $(*)$ mark the approximate positions of the triple points for $\beta\epsilon=20$ and 39, obtained by extrapolation.

$$\kappa\sigma\, e^{\kappa\sigma}=\beta U_0^{\mathrm{tp}}\lambda^{\mathrm{tp}}/\beta\epsilon \tag{11}$$

and use the second line of Eq. (7) to obtain η. The resulting line of triple points is denoted with the dashed line in Fig. 5, the diamonds highlight the triple points at $\beta\epsilon=8$, 20, 39, and 81, and the squares give the triple points used in our calculations. We see that the agreement between the two results (the squares and the diamonds) does not depend much on the value of $\beta\epsilon$ and therefore we can say that the position of the lower triple point is given precisely enough by the point Yukawa results.

It is also instructive to map our hard-core Yukawa phase diagrams in the $(\lambda,\beta U_0)$ and $(\lambda,\tilde{T})$ representations that are typically used to represent the phase diagram of point Yukawa particles. The mapping is given by Eqs. (7) and (8). The phase diagram in the $(\lambda,\tilde{T})$ representation is shown in Fig. 6: The solid lines are the point Yukawa results of Hamaguchi, Farouki, and Dubin [3] and the other lines are our hard-core Yukawa results. In the regions of the phase diagram in Fig. 6 where the lines from different $\beta\epsilon$ values fall on top of each other and on top of the point Yukawa lines, the presence of the effects of the hard-core interaction are minimal. This is especially true near the low $1/\kappa\sigma$ triple point region, located at $\lambda^{\mathrm{tp}}=6.90$ and $\tilde{T}^{\mathrm{tp}}=0.0038$ [3]. Moving from this triple point to larger values of λ, corresponding to decrease of $1/\kappa\sigma$, we see that the point Yukawa results for the fluid-fcc phase boundary stays between the fluid-fcc coexistence regions of the hard-core Yukawa results. Note that the fluid-fcc phase coexistence region looks very broad in this representation and that the tie lines are no longer horizontal. Moving away from the triple point along the fluid-bcc or the bcc-fcc line, we see that deviations from the point Yukawa limit appear sooner for smaller $\beta\epsilon$, as already mentioned.

In Fig. 7 we show the phase diagram in the $(\lambda,\beta U_0)$ representation plotted in linear-log scale. In this representation, the bcc-fcc and the fluid-fcc coexistence line from our hard-core Yukawa calculations behave as straight lines. This inspired us to estimate the position of the second, i.e., the high $1/\kappa\sigma$, triple point for $\beta\epsilon=20$ and $\beta\epsilon=39$ by simply extrapolating the coexistence lines and calculating the intercept point. The resulting approximate triple points are plotted in Fig. 7 with stars. After converting to the $(\eta,\kappa\sigma)$ plane using Eq. (7), they read $\eta=0.47$ and $\kappa\sigma=1.7$ for $\beta\epsilon=20$, and $\eta=0.57$ and $\kappa\sigma=1.0$ for $\beta\epsilon=39$.

Technical Details

The rest of this section is devoted to the technical details on calculating the phase diagrams and on the estimation of the error. The phase diagram for $\beta\epsilon=8$, shown in Fig. 1, was already in Ref. [5], and serves also as a check for the methods used. In order to obtain the phase diagram in Fig. 1, four Kofke integrations were started from the three positions given in Ref. [5], one from the hard-sphere limit with $p=11.5541$, $1/\kappa\sigma=0.0001$ $(\kappa\sigma=10\,000.0)$, $\eta_{\mathrm{fluid}}=0.491$, and $\eta_{\mathrm{fcc}}=0.543$, two from the lower triple point with $p=20.70$, $1/\kappa\sigma\approx0.156$ $[\kappa\sigma=6.4$, Eq. (11) predicts $\kappa\sigma=6.18]$, $\eta_{\mathrm{fluid}}=0.373$, $\eta_{\mathrm{bcc}}=0.379$, and $\eta_{\mathrm{fcc}}=0.380$, and one from the higher triple point with $p=44.1$, $1/\kappa\sigma\approx0.286$ $(\kappa\sigma=3.5)$, $\eta_{\mathrm{fluid}}=0.453$ and $\eta_{\mathrm{fcc}}=0.460$. In all the Kofke integrations the system sizes were $N_{\mathrm{fluid}}=256$, $N_{\mathrm{bcc}}=250$, and $N_{\mathrm{fcc}}=256$, and step size of $\Delta(\kappa\sigma)^{-1}=0.004$ was used. The thermodynamic averages needed in Eq. (4) were calculated by performing $N_s=10\,000$ NPT MC steps (trial moves per particle, or attempt to change the volume), both for the equilibration and for the production runs. When calculating the bcc-fcc coexistence, N_s was increased to 30 000.

The accuracy of the Kofke integration can be checked by measuring how the end points of the integration match with

the known results. In order to know the fluid-fcc coexistence at $1/\kappa\sigma=0.5$, free energy calculations were performed with system size $N_{\mathrm{fluid}}=N_{\mathrm{fcc}}=500$. Here and in all subsequent free energy calculations, 10 000 *NVT* MC steps for the equilibration and measurement runs were taken in order to calculate the ensemble averages, and ten integration points were used in the numerical integration using the Gaussian quadrature. In Fig. 1, the resulting fluid-fcc coexistence points are marked with circles. As Fig. 1 shows that the fluid-bcc, bcc-fcc, and low $1/\kappa\sigma$ fluid-fcc coexistence lines end up at the correct triple points, we expect that the errors in the corresponding Kofke integrations are small. However, at $1/\kappa\sigma=0.5$, the fluid-fcc coexistence points ($\eta_{\mathrm{fluid}}=0.486$ and $\eta_{\mathrm{fcc}}=0.495$) do not correspond exactly to the free energy results ($\eta_{\mathrm{fluid}}=0.476$ and $\eta_{\mathrm{fcc}}=0.485$), although the error, i.e., the difference in the packing fractions, is only about 1%. To check if the error is due to the difference in the system size, we redid the free energy calculation with the same system size as used in the Kofke integration, $N_{\mathrm{fluid}}=N_{\mathrm{fcc}}=256$. This resulted in fluid-fcc coexistence with $\eta_{\mathrm{fluid}}=0.469$ and $\eta_{\mathrm{fcc}}=0.477$, leading to an error of slightly less than 2% with respect to the Kofke integration result. Furthermore, since the result with the same system size does not correspond to the end point of the Kofke integration, we can conclude that the error is most likely due to an error in the position of the second triple point at $1/\kappa\sigma\approx 0.286$.

For the other phase diagrams with $\beta\epsilon$ = 20, 39, and 81, the location of the triple point, and hence the starting point of the Kofke integration, was obtained from Fig. 5 of Ref. [5]. For the phase diagram with $\beta\epsilon=20$ in Fig. 2, three Kofke integrations were started from $p=15.0$, $1/\kappa\sigma\approx 0.194$ [$\kappa\sigma=5.15$, while Eq. (11) predicts $\kappa\sigma=5.40$] with $\eta_{\mathrm{fluid}}=0.250$, $\eta_{\mathrm{bcc}}=0.2540$, and $\eta_{\mathrm{fcc}}=0.2543$. Note that while Fig. 5 of Ref. [5] gives only the pressure at the triple point, the packing fraction can be determined by performing a *NPT* MC simulation. The same system sizes, number of MC steps N_s, and $\Delta(\kappa\sigma)^{-1}$ were used as for the phase diagram with $\beta\epsilon=8$. The two check points at $1/\kappa\sigma=0.5$ and the fluid-bcc and the bcc-fcc coexistence points, were obtained using free energy calculations with system sizes $N_{\mathrm{fluid}}=N_{\mathrm{bcc}}=686$ and $N_{\mathrm{fcc}}=864$. As can be seen, the accuracy of the Kofke integration is good for the bcc-fcc coexistence line (error 1%) while the fluid-bcc line is slightly off (error 2%).

For the phase diagram with $\beta\epsilon=39$ in Fig. 3, the triple point is at $p=10.516$, $1/\kappa\sigma\approx=0.211$ [$\kappa\sigma=4.75$, Eq. (11) predicts $\kappa\sigma=4.84$] with $\eta_{\mathrm{fluid}}=0.1797$, $\eta_{\mathrm{bcc}}=0.1824$, and $\eta_{\mathrm{fcc}}=0.1827$. Again the same system sizes, number of MC steps N_s, and $\Delta(\kappa\sigma)^{-1}$ were used in the Kofke integration as for $\beta\epsilon=8$ and 20. We found that the bcc-fcc coexistence line, the Kofke integration, was stable until $1/\kappa\sigma\approx 0.32$. At higher values of $1/\kappa\sigma$ we found large fluctuations in η, denoting the breakdown of the Kofke integration. Only mild damping of the fluctuations were observed when the Kofke integration was repeated with a smaller step size $\Delta(\kappa\sigma)^{-1}=0.001$ (and with $N_s=15\,000$). In order to resolve the bcc-fcc coexistence line above $1/\kappa\sigma=0.32$, a starting point was determined by free energy calculations at $1/\kappa\sigma\approx 0.35$ ($\kappa\sigma=2.86$). The free energy calculations were performed for systems with $N_{\mathrm{bcc}}=700$ and $N_{\mathrm{fcc}}=768$ particles. The system size was increased in order to minimize the effect of the finite cutoff length. Note that with these system sizes the simulation box is not cubic but close to it. The resulting bcc and fcc packing fractions are $\eta_{\mathrm{bcc}}=0.4835$ and $\eta_{\mathrm{fcc}}=0.4837$ with pressure $p=240.318$. From this coexistence point, two Kofke integrations with the larger system sizes were performed towards lower and higher $1/\kappa\sigma$ with step sizes $\Delta(\kappa\sigma)^{-1}=0.002$ and $\Delta(\kappa\sigma)^{-1}=0.006$, respectively. The number of MC steps for both Kofke integrations was $N_s=20\,000$. For the Kofke integration going down in $1/\kappa\sigma$, large fluctuations were again seen near $1/\kappa\sigma=0.32$. In order to obtain a continuous phase diagram we connected the stable parts of the two Kofke integrations, one starting from the triple point and one starting from the bcc-fcc coexistence point determined by free energy calculations. Free energy calculations were performed at $1/\kappa\sigma=0.5$ for the fluid-bcc coexistence point ($N_{\mathrm{fluid}}=N_{\mathrm{bcc}}=432$) and as can be seen, the accuracy of the Kofke integration is adequate (error $<2\%$).

In the case of the phase diagram for $\beta\epsilon=81$, given in Fig. 4, the location of the triple point is at $p=7.242$ and $1/\kappa\sigma\approx=0.241$ [$\kappa\sigma=4.15$, Eq. (11) predicts $\kappa\sigma=4.24$] with $\eta_{\mathrm{fluid}}=0.1214$, $\eta_{\mathrm{bcc}}=0.1232$, and $\eta_{\mathrm{fcc}}=0.1234$. The same N_s and $\Delta(\kappa\sigma)^{-1}$ were used, as previously. Again, as for $\beta\epsilon=39$, the calculation of the bcc-fcc coexistence line was hindered because of a breakdown of the Kofke integration, which this time occurred close to $1/\kappa\sigma=0.4$. We noticed that above $1/\kappa\sigma=0.4$, in order to get rid of the effect of the finite cutoff, the system size should be increased dramatically. Therefore, instead of performing Kofke integrations with very large system sizes, we used free energy calculations at two points, at $1/\kappa\sigma\approx 0.42$ ($\kappa\sigma=2.4$) and at $1/\kappa\sigma=0.5$, and connected the two points in order to get an estimate of the bcc-fcc coexistence line. The free energy calculation at $1/\kappa\sigma\approx 0.42$ was done with the same parameters as for $\beta\epsilon=39$, except that the system size for the bcc was increased to $N_{\mathrm{bcc}}=800$ (resulting in an almost cubic simulation box). At $1/\kappa\sigma=0.5$, the system sizes were further increased to $N_{\mathrm{bcc}}=1024$ (cubic box) and $N_{\mathrm{fcc}}=972$ (almost cubic box).

IV. CONCLUSIONS

We determined the phase diagram of a system in which the particles interact with the hard-core repulsive Yukawa pair potential (1) with contact values $\beta\epsilon=8$, 20, 39, and 81. We compared the phase diagrams with those of the point Yukawa particles by mapping both systems onto each other. We showed that the difference between the phase behaviors of the hard-core repulsive Yukawa and point Yukawa particles reduces upon increasing the contact value $\beta\epsilon$, as might be expected. By comparing the phase diagrams, in more detail we determined the influence of the hard-core diameter more precisely. We found that the fluid-bcc coexistence line is well predicted by the point Yukawa phase diagram, while the high $1/\kappa\sigma$ bcc-fcc coexistence line deviates. The difference in the bcc-fcc coexistence line is caused by the hard-core repulsion that at high packing fractions ($\eta\gtrsim 0.5$) favors the fcc phase. The behavior of the bcc-fcc coexistence line for hard-core Yukawa particles gives rise to the second triple

point at high $1/\kappa\sigma$ (existence of which has already been reported in Ref. [5]), something that is missing from the phase diagram of point Yukawa particles. It was observed that with increasing $\beta\epsilon$, the second triple point escapes quickly to high values of $1/\kappa\sigma$ where, with the methods used in this study, the calculations are difficult to carry out. Because of this, our calculations reached the second triple point only for the lowest contact value $\beta\epsilon$; for two other values of $\beta\epsilon$ we estimated its position by extrapolation.

Our calculations explicitly included the determination of the phase coexistence regions. We observed that all the coexistence regions are very small, i.e., the difference between the densities of the coexisting phases is small. This was seen to be the case especially for the bcc-fcc coexistence. It was also observed that the coexistence regions become smaller with increasing contact values $\beta\epsilon$ of the hard-core Yukawa particles. Therefore, one might expect that the coexistence regions of highly charged colloids would be unmeasurably narrow, a statement that is not supported by all experimental observations [8,16,17].

In conclusion, we show that the phase diagram of hard-core repulsive Yukawa particles can be obtained for any contact value $\beta\epsilon$ which is sufficiently high ($\beta\epsilon=20$ or higher, corresponding to charge $Z>100$ for colloids with diameter $\sigma=100$ nm, suspended in water) by mapping the well-known phase boundaries of the point Yukawa particles given by fits (9) and (10) onto those of the hard-core repulsive Yukawa system using Eq. (7) and bearing in mind that the stable bcc region is bounded by a bcc-fcc coexistence at $\eta \approx 0.5$, i.e., the hard-core repulsion favors the bcc-fcc phase for $\eta > 0.5$.

ACKNOWLEDGMENTS

The authors would like to thank H. H. von Grünberg for useful discussions and P. Royall for critical reading of the manuscript. This work is part of the research program of the ''Stichting voor Fundamenteel Onderzoek der Materie (FOM),'' which is financially supported by the ''Nederlandse Organisatie voor Wetenschappelijk Onderzoek (NWO).'' We thank the Dutch National Computer Facilities foundation for access to the SGI Origin3800. The High Performance Computing group of Utrecht University is gratefully acknowledged for ample computer time. A.-P.H. gratefully acknowledges the financial support from the Finnish Cultural Foundation.

[1] B. Derjaguin and L. Landau, Acta Physicochim. URSS **14**, 633 (1941); E.J.W. Verwey and J.Th.G. Overbeek, *Theory of the Stability of Lyotropic Colloids* (Elsevier, Amsterdam, 1948).
[2] M.O. Robbins, K. Kremer, and G.S. Grest, J. Chem. Phys. **88**, 3286 (1988).
[3] S. Hamaguchi, R.T. Farouki, and D.H.E. Dubin, Phys. Rev. E **56**, 4671 (1997).
[4] E.J. Meijer and F. El Azhar, J. Chem. Phys. **106**, 4678 (1997).
[5] F. El Azhar, M. Baus, J.-P. Ryckaert, and E.J. Meijer, J. Chem. Phys. **112**, 5121 (2000).
[6] S. Alexander, P.M. Chaikin, P. Grant, G.J. Morales, and P. Pincus, J. Chem. Phys. **80**, 5776 (1984).
[7] E. Trizac, L. Bocquet, and M. Aubuoy, Phys. Rev. Lett. **89**, 248301 (2002).
[8] Y. Monovoukas and A.P. Gast, J. Colloid Interface Sci. **128**, 533 (1989).
[9] D.A. Kofke, Mol. Phys. **78**, 1331 (1993); J. Chem. Phys. **98**, 4149 (1993).
[10] D. Frenkel and B. Smit, *Understanding Molecular Simulations*, 2nd ed. (Academic Press, New York, 2002).
[11] D. Frenkel and A.J.C. Ladd, J. Chem. Phys. **81**, 3188 (1984).
[12] G. Salin and J.-M. Caillol, J. Chem. Phys. **113**, 10 459 (2000).
[13] R.T. Farouki and S. Hamaguchi, J. Comput. Phys. **115**, 276 (1994).
[14] E.L. Pollock and J.P. Hansen, Phys. Rev. A **8**, 3110 (1973).
[15] To put this in context, note that the density jump for the fluid-fcc coexistence of the hard spheres is around 10%.
[16] E.B. Sirota, H.D. Ou-Yang, S.K. Sinha, P.M. Chaikin, J.D. Axe, and Y. Fujii, Phys. Rev. Lett. **62**, 1524 (1989).
[17] H.J. Schöpe, T. Decker, and T. Palberg, J. Chem. Phys. **109**, 10 068 (1998).